THEORETICAL ANALYSIS OF BUILDING HEIGHT ESTIMATION USING SPACE-BORNE SAR-INTERFEROMETRY FOR RAPID MAPPING APPLICATIONS

Stefan Hinz[1], Sarah Abelen[2]

[1]Institute of Photogrammetry and Remote Sensing, Univeristät Karlsruhe, Kaiserstr. 12, 76 128 Karlsruhe
[2]Remote Sensing Technology, Technische Universität München, Arcisstr. 21, 81 333 München
Stefan.Hinz@ipf.uni-karlsruhe.de

Commission III, WG 5

KEY WORDS: Space-borne Interferometric SAR, Building Heights, TanDEM-X, CosmoSkymed

ABSTRACT:
The great potential of space-borne SAR images for semi- or fully-automatic mapping of topographic features has been shown by many approaches. While most of them focus on 2D mapping of topographic features, some preliminary research on the complex task of automatic delineation of 3D information in urban environments has been initiated in recent years. In this paper, we analyze the capabilities of new space-borne interferometric SAR missions – in particular the German TanDEM-X mission – with respect to their potential of deriving building heights. To this end, we summarize the mathematical framework and carry out a thorough analytical accuracy analysis involving various sensor and scene parameters.

1. INTRODUCTION

The new class of space-borne high resolution SAR sensors such as TerraSAR-X, SAR-Lupe or Cosmo-SkyMed is able to provide SAR images of 1-3m spatial resolution or even below in special spotlight modes. Naturally, the development of methods to automatically derive detailed cartographic information from this kind of data is a major issue driven by these missions. Since SAR is largely independent from illumination and weather conditions, it is furthermore an attractive imaging technology for acquiring area-wide information of regions hit by disasters such as floodings, landslides, or earthquakes.

The great potential of space-borne SAR images for semi- or fully-automatic mapping of 2D topographic features has been shown by many encouraging approaches, e.g., (Negri et al., 2006; Frey & Butenuth, 2009) for delineation of roads and (Jäger et al. 2007; Hänsch & Hellwich, 2008) for classification of agricultural features, just to name few recent ones. The derivation of 3D features is however more difficult, since these current civilian space-borne systems have only limited interferometric capabilities. While the acquisition of along-track interferometric image pairs is possible by programming special RADAR imaging modes (e.g. DRA mode or Aperture Switching mode for TerraSAR-X (Runge et al., 2006)) enabling the detection of moving objects (Suchandt et al., 2008; Weihing et al., 2008), none of the current civilian space systems is equipped with an across-track interferometer, which would provide the basis for deriving topographic heights (Bamler & Hartl, 1998; Cumming & Wong, 2005). The necessary across-track baseline is only given when forming an interferogram of two SAR acquisitions taken from the same orbit yet at different passes of the satellite, and thereby relying on the positional variation of the orbits. It is clear that the resulting interferograms suffer from decorrelation depending on temporal variability of the objects under investigation.

This situation will change once TerraSAR-X will be accompaigned by a second, quasi-identical SAR satellite in late 2009, leading to the TanDEM-X mission. Both satellites will fly almost in parallel forming a helix-like orbit pair (Zink et al. 2006). This configuration allows to acquiring SAR image pairs with variable across-track geometry resulting in a significantly improved interferometric coherence. The great benefit of single-pass across-track SAR interferometers has been intensively studied in the context of the Shuttle Radar Topography Mission (SRTM). Despite of the limited spatial resolution of SRTM data (approx. 25m), it was possible to compute a global digital elevation model with standardized height accuracy of few meters, see, e.g., the comprehensive overview given in (Rabus et al., 2003).

TanDEM-X will deliver high coherence interferometric data of the meter class. Although the mission is mainly designed to generate accurate digital elevation models satisfying HRTI-3 standards (Zink et al., 2006), it can be expected that this kind of data opens up a much wider field for specialized methods for 3D mapping of topographic features. The automated derivation of building heights or even the detailed reconstruction of buildings is certainly an important application amongst these.

Apart from the improved spatial resolution, a major difference between TanDEM-X and SRTM is the variable across-track baseline of TanDEM-X, whereas the baseline of SRTM was held quasi-constant due to the second antenna mounted at a 60m boom (and neglecting periodic baseline variations as consequence of thrusting). Hence, a thorough analysis of accuracy aspects of height estimation under the given flexibility of TanDEM-X is a key issue.

Following questions should be answered by the analysis:

- Which accuracy level in terms of building height estimation can be reached with interferometric data as it will be provided by TanDEM-X?
- Is this accuracy sufficient to derive object specific information for rapid mapping in the context of crisis management? Such information may comprise, e.g.,
    - the number of floors to estimate the amount of people living in a house
    - attached building parts of different height
    - the roof type (flat roof, saddle roof, etc.)
- How would the accuracy improve, if external data from GIS is included (e.g. digital building footprints)?

The reminder of this paper is organized as follows: Section 2 gives a brief review of state-of-the-art methods for delineating the 3D geometry of buildings from SAR images in general, eventually leading to a discussion of the boundary conditions of this study. The theoretical background for height estimation from across-track interferometry as well as error sources are compiled in Section 3, before Section 4 analyses the accuracy potential of deriving building heights under various given prerequisites. Finally, Section 5 draws conclusions in the light of the TanDEM-X mission and the results of this study.

2. 3D BUILDING GEOMETRY FROM SAR IMAGES

2.1. Overview

Over the past decades, a large variety of approaches for deriving 3D building information from SAR images has been developed. According to underlying methods and used data the different methods can be roughly grouped into following categories:

(a) height-from-shadow using mono- or multi-aspect data
(b) fitting prismatic models based on statistical optimization
(c) model-driven segmentation of pre-computed height data
(d) height estimation supported by feature detection / matching
(e) Exploiting layover areas in single or multiple InSAR pairs

To keep the overview focused, we only refer to the original work of each of these groups. We are aware that numerous approaches have been developed meanwhile, which could be assigned to one or more of these groups.

Ad a) Due to the oblique imaging geometry of SAR systems, buildings cause the well-known RADAR shadow, which basically corresponds to the occluded area at ground. As for conventional optical shape-from-shadow approaches, it only needs simple trigonometry to calculate the object height from the shadow boundary when knowing the sensor imaging geometry and assuming horizontal ground (similar for the layover area (Tupin, 2003)). A compilation of the corresponding formulae can be found, for instance, in (Sörgel et al. 2006). It is usually assumed that a shadow edge corresponds to a certain object edge, whose height is to be estimated. As only a few number of building edges can be matched to shadow edges for a specific viewing direction of the SAR, (Bolter & Leberl, 2000; Leberl & Bolter, 2001) generalize this approach to multi-aspect SAR and embed it into an iterative height estimation framework supported by InSAR cues. By this, building footprint and height are estimated simultaneously, yielding an accuracy of 1.5m – 2m for airborne SAR.

Ad b) The concept described in (Quartulli & Datcu, 2001; 2003) models the geometry of buildings and geometric relations between adjacent buildings by a number of parameters (position, length, width, height, roof slope, distance etc.). After initialization of model instances in image space, the parameters are statistically optimized using amplitude, coherence and interferometric phase information from the images. While this kind of thorough object-oriented modeling helps to cope with heavy noise and image derogations, it limits the approach to a small number of building shapes, not speak about the computational complexity mandatory for parameter optimization. This might one of the reasons why the results cannot prove the general feasibility of the approach and no accuracy analysis has been carried out; whereas, the mathematical formulation is very elegant.

Ad c) A purely data-driven strategy that complements the aforementioned approach is presented in (Gamba & Houshmand, 1999; Gamba et al., 2000). The procedure starts with the computation of the interferogram and derives level lines by segmenting it into height intervals. Level lines fulfilling certain shape constraints are selected as seed points to start a regiongrowing algorithm. This algorithm continues as long as segments can be added without exceeding a predefined threshold for co-planarity. The achieved accuracy using airborne C-band data is reported to be 2.5m for large industrial buildings. This method is in principle independent of the data source and can be applied to any kind of height models, as so for LIDAR-based height models (Gamba & Houshmand, 2000).

Ad d) While the former extraction strategy infers the semantics of buildings purely based on the roof geometry, approaches following the spirit of (Sörgel et al., 2003; Tison et al., 2007) include hypotheses of buildings, building parts, and/or adjacent context objects (roads, vegetation, etc.) from the very beginning of processing. To this end, a supervised classification and/or feature detection is carried out before building reconstruction. This may contain areal objects but also linear features and spots indicating double bounces at building walls, which become especially prominent in high resolution SAR (Stilla, 2007). The cues provided by these hypotheses are then iteratively grouped and optimized together with the heights derived from InSAR data until reasonably shaped buildings are extracted or hypotheses are rejected. Due to generic processing of multiple cues, this concept is easily extended to multi-aspect SAR data. The reported accuracy yields again 2 – 3m for the airborne case.

Ad e) The final group of approaches does not only include image features derived from SAR or InSAR data but models the complete interferometric phase profile for building walls and roofs (Thiele et al., 2007). Since vertical walls form layover areas as consequence of the oblique RADAR distance measurement, this kind of modelling implicitly contains the assumption that the main contribution of scattering in such layover areas is induced by building walls and not by clutter in front of the building or by the overlayed part of the roof. This approach can be generalized to SAR tomography (Reigber & Moreira, 2000; Fornaro et al., 2003) if more than one interferometric pair of the same viewing direction is available. (Zhu et al., 2008; 2009) show that deriving 3D information via tomographic analysis and statistical model selection can be adapted to pixelwise calculation of dense height maps of urban areas, thus linking the concepts of SAR tomography with Persistent Scatterer Interferometry (Ferretti et al., 2001; Kampes, 2006). These approaches are however in a preliminary stage so that a thorough accuracy analysis is not yet available.

2.2 Discussion

While each of the approaches is characterized by individual advantages and limitations, the latter category seems to be a good compromise between a data-driven strategy and object-oriented modeling. It is flexible in the sense that it is not restricted a-priori to specific building shapes. On the other hand, there are still object-oriented aspects included since typical building regularities are to identify in the InSAR data.

Concerning the utilization of shadow and layover effects one has to keep in mind that, especially in urban areas, layover appears very often and may also cover shadow from neighboring buildings. Hence, shadow areas are usually hard to

identify automatically, while layover areas still carry useful information, even if this is embedded in clutter (see the example of a repeat-pass TerraSAR-X interferogram in Figure 1). Moreover, the incorporation of additional knowledge about buildings may help to separate useful signal from clutter, especially as buildings have regular shapes and, often, digital maps indicating the building footprints are available.

Multi-baseline and multi-aspect approaches show great potential to reconstruct buildings with high accuracy and level of detail. However, the time needed to acquire the necessary images is usually too long for rapid mapping, especially in the context of providing crisis information. Consequently, the analysis in Section 3 concentrates on accuracy aspects of single-pass interferometry. The building heights are expected to be computed from the interferometric signal of layover regions. The inherent contribution of clutter in these areas is accommodated by some loss of interferometric coherence, which is also taken into account for the final height accuracy.

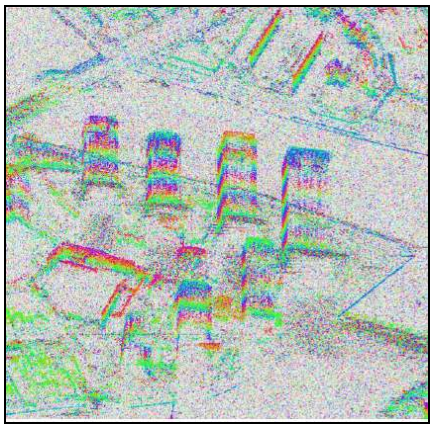

Figure 1: Interferometric fringes in layover area of tall buildings computed from dual-pass TerraSAR-X interferogram (courtesy M.Eineder, DLR).

3. HEIGHT ACCURACY OF INSAR MEASURMENTS – THEORY

In this section we revise the mathematical theory for relating specific sensor and scene parameters with the desired height accuracy for the case of space-borne SAR. A detailed derivation of the formulae can be found in (Bamler & Schättler, 1993; Bamler & Hartl, 1998; Cumming & Wong, 2005). Figure 2 (left) depicts the typical geometric configuration of across-track interferometry. The phase values of the two acquisitions can be derived from the well-known two-way range equation

$$\phi_1 = -\frac{2\pi}{\lambda} 2R + \phi_{scatt,1} \tag{1}$$

$$\phi_2 = -\frac{2\pi}{\lambda} 2\left(R + \Delta R\right) + \phi_{scatt,2} \tag{2}$$

where ϕ_1 and ϕ_2 are the SAR phases at a certain pixel, λ is the wavelength, R is the range between one antenna and the point on ground in viewing direction θ, and ΔR is the range difference induced by the baseline vector B and its component perpendicular to the viewing direction $B_\perp$, respectively. Under the assumption that the unknown phase contributions caused by random scattering $\phi_{scatt,1}$ and $\phi_{scatt,2}$ are identical

$$\phi_{scatt,1} \equiv \phi_{scatt,2} \tag{3}$$

one can express the interferometric phase ϕ for a certain point by

$$\phi = \phi_1 - \phi_2 = \frac{4\pi}{\lambda} \Delta R \tag{4}$$

In order to convert the this phase into height values z, it is useful to first formulate the functional relationship between ΔR and the direction perpendicular to R on ground, ζ (see Figure 2 (right)):

$$\zeta \cong -\frac{R_S}{B_\perp} \Delta R = -\frac{R_S}{B_\perp} \frac{\lambda}{4\pi} \phi \tag{5}$$

Solving for ϕ and projecting into the vertical direction z yields

$$\phi \cong -\frac{4\pi}{\lambda} \frac{B_\perp}{R} \frac{z}{\sin\theta} \tag{6}$$

Equation (6) is the basis to calculate the so-called phase-to-height sensitivity:

$$\frac{\partial\phi}{\partial z} = -\frac{4\pi}{\lambda} \frac{B_\perp}{R\sin\theta} \tag{7}$$

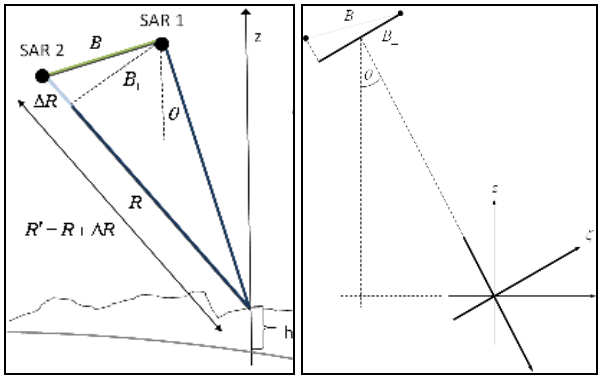

Figure 2: Geometric layout of across-track interferometry (left) and definition of local co-ordinate system on ground, ζ, (right).

Figure 3 illustrates the influence of varying incidence angle and baseline length on the phase-to-height-sensitivity. As can be seen, the interferometric measurement gets more and more sensitive the longer the baseline and the smaller (steeper) the incidence angle is.

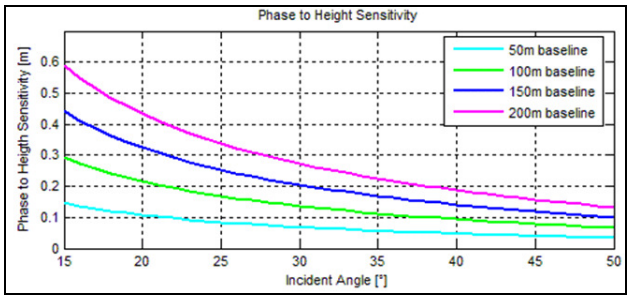

Figure 3: Influence of incidence angle and baseline on phase-to-height-sensitivity

In practice, the identity of Eq. (3) does not hold strictly, neither for ideal single-pass interferometers. Reasons therefore are varying bi-directional scattering, varying volume scattering, thermal noise, etc. However, a guess about the similarity of the two complex-valued SAR images u_1 and u_2 can be computed for each pixel $[i,k]$ by the coherence estimate $|\gamma| = |\hat{\gamma}[i,k]|$ calculated in a predefined local neighbourhood W:

$$|\gamma| = |\hat{\gamma}[i,k]| = \frac{\left|\sum_W u_1[i,k]\,u_2^*[i,k]\right|}{\sqrt{\sum_W |u_1[i,k]|^2 \sum_W |u_2[i,k]|^2}} \tag{8}$$

Based on the coherence estimate one can derive the probability density distribution (pdf) of the interferometric phase $\mathrm{pdf}(\phi; L)$ of the expectation $\bar{\phi}$ depending on the number of looks L, i.e. the amount of averaging independent pixels (Lee et al., 1994):

$$\mathrm{pdf}(\phi; L) = A(\phi; L) + B(\phi; L) \tag{9}$$

with

$$A(\phi; L) = \frac{\Gamma(L+1/2)\left(1-|\gamma|^2\right)^L |\gamma| \cos(\phi-\bar{\phi})}{2\sqrt{\pi}\;\Gamma(L)\left(1-|\gamma|^2\cos^2(\phi-\bar{\phi})\right)^{L+1/2}},$$

$$B(\phi; L) = \frac{\left(1-|\gamma|^2\right)^L}{2\pi}\;{}_2F_1\left(L, 1; 1/2; |\gamma|^2\cos^2(\phi-\bar{\phi})\right)$$

and $\Gamma(x) = (x-1)!$ being the Gamma function and ${}_2F_1(a,b;c;z)$ being the hypergeometric Gaussian function. Figure 4 shows the shape of Eq. 9 for a fixed coherence and varying averaging while, in Figure 5, averaging is fixed and coherence varies.

Although the pdf of the interferometric phase is not strictly Gaussian, it can be seen from the functions displayed in Figures 4 and 5 that the pdf's first- and second-order moment ($\bar{\phi}$ and σ_ϕ) carry the most information of this distribution. Furthermore, assuming that $\phi(z)$ is locally linear, one can write after Taylor expansion of $\phi(z)$ and omitting higher order terms:

$$\frac{\partial\phi}{\partial z} = \frac{\Delta\phi}{\Delta z} \tag{10}$$

Computing σ_ϕ numerically from Eq. 9 and inserting $\Delta\phi = \sigma_\phi$ and $\Delta z = \sigma_z$ into Eq. 10 yields finally the standard deviation of the height estimates:

$$\sigma_z = \frac{\sigma_\phi}{\partial\phi/\partial z} \tag{11}$$

Figure 6 visualizes the behaviour of the standard deviation of the interferometric phase for varying coherence and number of looks. An evident feature of this function is the large influence of averaging for moderate coherence values. Only four looks, for instance, improve the standard deviation approximately by 50% at a coherence of 0.65. Figure 7 shows typical height distributions for varying coherence and a specific fixed set of sensor parameters.

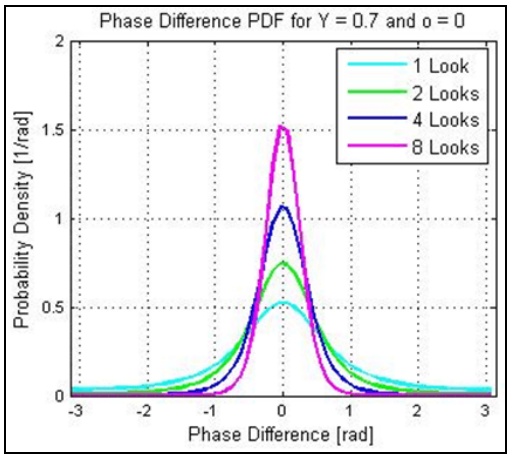

Figure 4: pdf of interferometric phase for fixed coherence and varying averaging.

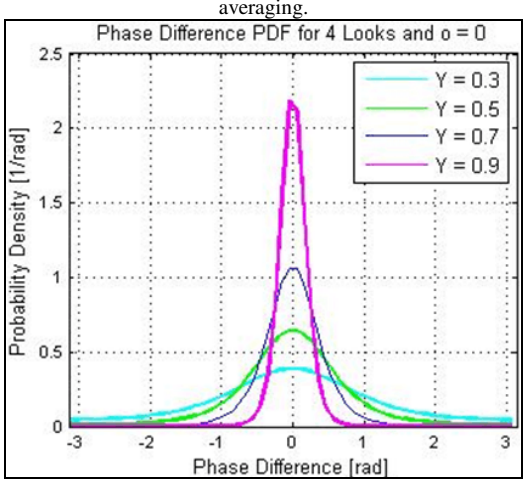

Figure 5: pdf of interferometric phase for fixed averaging and varying coherence.

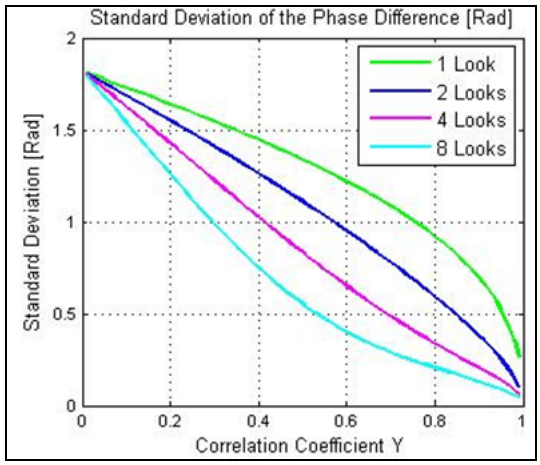

Figure 6: Standard deviation of interferometric phase for varying coherence and number of looks.

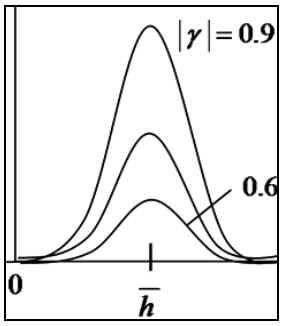

Figure 7: pdf of height for varying coherence (other parameters fixed).

4. ACCURACY OF BUILDING HEIGHT ESTIMATION

The accuracy assessment has been carried out with the scheme described above. Parameter values were chosen in accordance to the main TanDEM-X specifications. Mutual influence of following parameters has been investigated:

- baseline length
- incidence angle
- coherence
- amount of averaging/smoothing
- wavelength

Figure 8 exemplifies the specific case of moderate coherence (0.6) and only one single look, i.e. the original spatial resolution is maintained and no smoothing is done. A low coherence has been chosen by intention, although significantly better values are expected for TanDEM-X, since clutter may decrease the coherence in layover areas. The ideal case for this configuration suggests to selecting a long baseline (e.g. 150m) and a steep incidence angle (15°), which results in a height accuracy of approx. 2.5m. Incidence angles less close to the system limits would yield an accuracy of 5m – 7m.

The effect of improving coherence is illustrated in Figure 9, where height accuracy is plotted against coherence and various baselines. It can be seen that, for a baseline of 150m, height accuracy increases from 2.5m at a coherence of 0.6 up to 1.5m at a coherence of 0.9.

The final assessment deals with the influence of the number of looks. A coherence of 0.7 for the case of 200m baseline and 15° incidence angle enables the derivation of building heights with 1m accuracy for the given viewing geometry (see Figure 10). As this kind of averaging reduces the spatial resolution, it is reasonable to investigate the effect of smoothing onto the height accuracy only up to four looks. What is moreover evident from Figure 10 is that the increase of height accuracy is significant from one to two and three looks, but it is then gradually attenuating – especially for typical coherence values in the range of 0.6 – 0.8.

As a last remark we refer to the used wavelength (X-band in our calculations). Equation 7 shows that the RADAR wavelength is a constant factor for the phase-to-height-sensitivity, which directly propagates to the standard deviation of height measurements. A longer wavelength (L-band for instance) yields a worse phase-to-height sensitivity and consequently a worse height accuracy. It should be noted, however, that long wavelengths generally yield better interferometric coherence depending on the scene characteristics. Hence, this effect could be partly compensated.

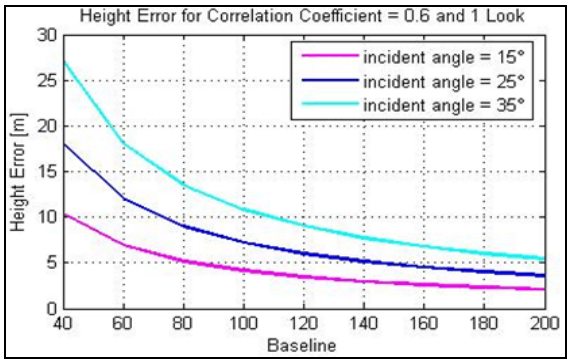

Figure 8: Height accuracy for varying baseline and incidence angle while other parameters are fixed.

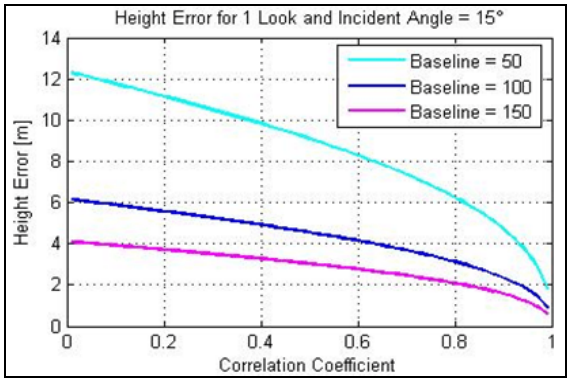

Figure 9: Height accuracy for varying baseline and coherence while other parameters are fixed.

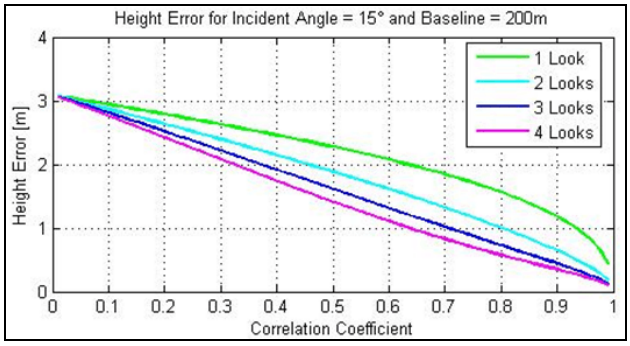

Figure 10: Height accuracy for varying looks and coherence while other parameters are fixed.

5. DISCUSSION AND CONCLUSION

The above analysis shows that space-borne interferometric SAR systems like TanDEM-X will allow to measure vertical heights with a standard deviation of roughly 1.5m, which also holds for the case of moderate coherence in layover areas. Regarding the application of rapid mapping, this accuracy will certainly allow the estimation of the number of floors or the detection of changes in the 3D building geometry. However, baselines and incidence angles have to be chosen carefully, as they are close to the technical limits (i.e. “critical baseline” and steep viewing angle). These constraints can be relaxed when additional data in form of digital ground plans is available. These allow, for instance, the utilization of specialized filters instead of simple multi-looking. The geometry of the filter mask can then be adapted to the respective building shape to include as much pixels as possible as observations into the height measurement. Recall Figure 6 to see how the standard deviation of interferometric phase improves with increasing number of observations.

Further research will include investigations of the validity of Eq. 10 in real scenarios, e.g. by calculating the accuracy of heights based on phase differences while the phase estimate for the ground may have better accuracy than those of walls and roof. Another line of research could be the use of explicit models for scatterers typically appearing at buildings, instead of modeling their influence only implicitly by a lower coherence.

REFERENCES

Bamler, R., Hartl, P., 1998. Synthetic aperture radar interferometry. Inverse Problems: pp. R1 – R54.

Bamler, R., Schättler, B., 1993. SAR geocoding. Wichmann, Karlsruhe, chapter 3, pp. 53 – 102.

Bolter, R., Leberl, F., 2000. Phenomenology-based and interferometry-guided building reconstruction from multiple SAR images, Proc. of EUSAR 2000, pp. 687–690.

Cumming, I., Wong, F., 2005. Digital Processing of Synthetic Aperture Radar Data, Artech House, Boston, 2005.

Ferretti, A., Prati, C., Rocca, F, 2001. Permanent scatterers in SAR interferometry. IEEE Transactions on Geoscience and Remote Sensing, 39, 8-20

Fornaro, G., Serafino, F., Soldovieri, F., 2003. Three-dimensional focusing with multipass SAR data. IEEE Transactions on Geoscience and Remote Sensing, 41, 507-517

Frey, D., Butenuth, M., 2009. Analysis of Road Networks after Natural Disasters using Multi-sensorial Remote Sensing Techniques. In: Eckhard, Seyfert (eds.), Publikationen der Deutschen Gesellschaft für Photogrammetrie, Fernerkundung und Geoinformation 18, in press.

Gamba. P., Houshmand, B., 1999. Three dimensional urban characterization by IFSAR measurements, Proc. Of IGARSS'99, pp. 2401–2403.

Gamba. P., Houshmand, B., 2000. Digital surface models and building extraction: A comparison of IFSAR and LIDAR data, IEEE Transactions on Geoscience and Remote Sensing 38(4): 1959–1968.

Gamba. P., Houshmand, B., Saccani, M., 2000. Detection and extraction of buildings from interferometric SAR data, IEEE Transactions on Geoscience and Remote Sensing 38(1): 611–617.

Hänsch, R., Hellwich, O. 2008. Weighted Pyramid Linking for Segmentation of Fully-Polarimetric SAR Data, International Archives of Photogrammetry, Remote Sensing and Spatial Information Sciences 37(/B7a), pp. 95-100

Jäger, M., Neumann, M., Guillaso, S., Reigber, A., 2007. A Self-Initializing PolInSAR Classifier Using Interferometric Phase Differences, IEEE Transactions on Geoscience and Remote Sensing 45(11): 3503-3518.

Kampes, B. M., 2006. Radar Interferometry – The Persistent Scatterer Technique. *Springer*-Verlag, Berlin, Germany.

Leberl, F., Bolter, R., 2001. Building Reconstruction from Synthetic Aperture Radar Images and Interferometry. In: Baltsavias, E., Grün, A., van Gool, L. (eds.): Automatic Extraction of Man-Made Objects from Aerial and Space Images (III). Balkema Publishers, Lisse, The Netherlands.

Lee, J-S., Hoppel, K., Mango, S., Miller, A., 1994. Intensity and phase statistics of multilook polarimetric and interferometric SAR imagery IEEE Transactions on Geoscience and Remote Sensing 32: 1017–28

Negri, M., Gamba, P., Lisini, G., Tupin, F., 2006. Junction-Aware Extraction and Regularization of Urban Road Networks in High Resolution SAR Images. *IEEE Transactions on Geoscience and Remote Sensing* 44(10): 2962-2971.

Quartulli, M., Dactu, M. 2001. Bayesian model based city reconstruction from high resolution ISAR data, IEEE/ISPRS Joint Workshop on Remote Sensing and Data over Urban Areas, on CD

Quartulli, M., Datcu, M., 2003. Stochastic modelling for structure reconstruction from high-resolution SAR data, Proc. of IGARSS'03, pp. 4080–4082.

Rabus, B., Eineder, M., Roth, A., Bamler, R., 2003. The Shuttle Radar Topography Mission (SRTM) – A New Class of Digital Elevation Models Acquired by Spaceborne Radar. ISPRS Journal of Photogrammetry & Remote Sensing 57(4): 241 - 262

Reigber, A., Moreira, A., 2000. First demonstration of airborne SAR tomography using multibaseline L-band data. IEEE Transactions on Geoscience and Remote Sensing, 38, 2142-2152

Runge, H., Laux, C., Metzig, R., Steinbrecher, U., 2006. Performance Analysis of Virtual Multi-Channel TS-X SAR-Modes. Proceedings of EUSAR'06, Dresden, Germany, on CD.

Sörgel, U., Thoennessen, U., Stilla, U., 2003. Iterative building reconstruction from multi-aspect InSAR data," ISPRS Archives of Photogrammetry, Remote Sensing and Spatial Information Sciences, vol. 34.

Sörgel, U., Thoennessen, U., Brenner, A., Stilla, U., 2006. High-resolution SAR data: new opportunities and challenges for the analysis of urban areas. Radar, Sonar and Navigation, IEE Proceedings 153, 294-300

Stilla, U., 2007. High Resolution Radar Imaging of Urban Areas, Photogrammetric Week, Wichmann-Verlag, pp. 149–158

Suchandt, S., Runge, H., Breit, H., Kotenkov, A., Weihing, D., Hinz, S., Palubinskas, G., 2008. Traffic Measurements with TerraSAR-X: Processing System Overview and First Results. In: Proceedings of EUSAR '08, Friedrichshafen, Germany, on CD.

Thiele, A., Thoennessen, U., Cadario, E., Schulz, K., Soergel, U. 2007. Building Recognition from Multi-Aspect High Resolution InSAR Data in Urban Areas. In: IEEE Transactions on Geoscience and Remote Sensing 45 (11): 3583-3593.

Tison, C., Tupin, F., Maitre, H. 2007. A fusion scheme for joint retrieval of urban height map and classification from high resolution interferometric SAR images, IEEE Transactions on Geoscience and Remote Sensing 45(2): 495–505.

Tupin, F., 2003. Extraction of 3D information using overlay detection on SAR images, GRSS/ISPRS Joint Workshop on "Data Fusion and Remote Sensing over Urban Areas", pp. 72–76.

Weihing, D., Suchandt, S., Hinz, S., Runge, H., Bamler, R., 2008. Traffic Parameter Estimation Using TerraSAR-X Data. In: International Archives of Photogrammetry, Remote Sensing and Spatial Geoinformation Sciences, Vol 37(B7), pp. 153 – 156.

Zhu, X., Adam, N., Bamler, R., 2008. First Demonstration of Space-borne High Resolution SAR Tomography in Urban Environment Using TerraSAR-X Data. Proceedings of CEOS SAR Workshop on Calibration and Validation

Zhu, X., Adam, N., Bamler, R., 2009. Space-borne High Resolution SAR Tomography: Experiments in Urban Environment Using TerraSAR-X Data. Proc. of URBAN 2009, Shanghai, CN, to appear.

Zink, M., Fiedler, H., Hajnsek, I., Krieger, G., Moreira, A., Werner, M., 2006. The TanDEM-X Mission Concept. Proc. of IGARSS 2006, on CD